The dynamics of interface relaxation and destratification in AgNi multilayers



1994 J. Phys.: Condens. Matter 6 1099

(http://iopscience.iop.org/0953-8984/6/6/014)

J. Phys.: Condens. Matter 6 (1994) 1099–1112. Printed in the UK

# The dynamics of interface relaxation and destratification in AgNi multilayers

V Pelosin, J Hillairet and B Rodmacq

CEA/Département de Recherche Fondamentale sur la Matière Condensée, SP2M/MP, 85X, 38041 Grenoble Cédex, France

Received 23 August 1993

**Abstract.** Resistance and length changes were measured during thermal treatments on free-standing AgNi multilayers. The experiments allowed a clear separation of the successive stages of the microstructural evolution of these stratified structures: interfacial relaxation, destratification and grain growth. The kinetics of these processes were extracted by monitoring resistivity and length during thermal cycles and isotherms. A substantial densification was revealed during the interface relaxation, that results in a slowing down of the local reorganization process. An early diffusional creep was also shown; its occurrence is restricted to the destratification region.

## 1. Introduction

In recent years basic research as well as technology have focused much interest on the study of the physical properties of metallic multilayers and superlattices in relation to superperiodicity, and also to interface structure. Much fewer investigations have dealt with modifications of the latter that occur on aging or controlled annealing, although these changes may considerably alter properties of technological interest, such as electronic transport or magnetoresistance.

The purpose of this paper is to investigate the time and temperature scale of the successive stages of microstructural evolution occurring during thermal treatments and to determine the related kinetics. The selected AgNi system is characterized by negligible mutual solubility and large (15%) lattice mismatch of the constituents. As will be shown below, by obtaining free-standing samples we were allowed to study the behaviour of the multilayer films when these were submitted to temperature cycles. This could be done without the disturbing influence of thermoelastic stresses that would have inherently been generated in supported samples. Taking advantage of this, resistance, and also length and creep measurements, could be performed. The observations cover a broad temperature range that extends from 300 K to about 1000 K.

## 2. Experimental

The AgNi multilayer samples were prepared in a DC triode sputter deposition system. The sputtering pressure was $6 \times 10^{-4}$ Torr of argon gas and the deposition rate was about 0.1 nm $s^{-1}$. An equal number of monolayers of each constituent was deposited for every elemental stratum. In the following, the thickness of the elemental strata will be referred

0953-8984/94/061099+14$07.50  

to in numbers of atomic planes per stratum. The rotating substrate holder was cooled by a liquid nitrogen flow such that the deposition temperature was around 100 K. Total thicknesses were generally 5 micrometers and, occasionally, a few hundred nanometres. At the larger thicknesses, the samples detached spontaneously from their substrate when air pressure was readmitted in the sputtering chamber after completion of the deposition. Some samples were also deposited at ambient temperature, but they remained attached to their glass substrate. The surface dimensions of the samples were $2.8 \times 22$ mm$^2$.

X-ray diffraction was performed in both standard symmetrical reflection and transmission geometries. The recorded spectra, together with high-resolution electron microscopy, showed that superlattices with sharp interfaces are formed in a broad range of bilayer periods, down to $Ag_2Ni_2$ and $Ag_3Ni_3$ for the samples prepared at liquid nitrogen or ambient temperature, respectively [1, 2]. Magnetization measurements confirmed the existence of sharp interfaces [3]. These superlattices are polycrystalline with both Ag and Ni strata exhibiting a well defined (111) texture parallel to the growth direction. The grain size was estimated from the x-ray transmission experiments to lie in the nanometre range, and gets larger as the period is increased.

The in-plane resistivity was first measured at the reference temperature of 300 K, using a conventional four-probe method, with a 100 nV resolution voltmeter determining the voltage drop for a constant 10 mA DC current. For this purpose, the specimens were equipped with platinum potential leads spot-welded 10 mm apart from each other. For the thermal treatments and simultaneous measurements, the samples were put in a cryostat surmounted with a furnace. The temperature cycles were conducted entirely in the vapours emanating from a liquid helium bath under normal pressure. They mostly consisted of successive heating and cooling runs at a rate of 2 K min$^{-1}$, or in long-duration isotherms, or else in step-wise short-time temperature anneals.

For the dilatometric and creep measurements, the samples, of free length 15.6 mm, were disposed vertically on a specially designed balance system [4]. Their lower part was fixed, while their upper end was rigidly connected to the mobile arm of the balance and to a plateau moving freely in a cylindrical cavity. The whole assembly was placed in a chamber, which was evacuated and then filled with argon gas, at a pressure of 2 mbar. Temperature cycles were then performed with the use of a low-inertia furnace. In the stable regime, temperature control was better than 0.1 K. Heating and cooling rates were usually 2 K min$^{-1}$. The modifications in specimen length induced by thermal variations or by structural changes were inferred from the variations in the absorption frequency of this resonant cavity set-up using a microwave technique. These modifications are directly proportional to the variations of frequency. The resolution was 2 nm, that is one part in $10^7$, given the free length of the specimens studied. The stability was better than 20 nm over several hours. From a technical standpoint, each end of the samples was glued to a flat portion of a silica rod using a zirconium cement. For the dilatometric measurements, a small stress of the order of $10^{-2}$ N was applied to straighten the film and suppress its eventual camber. For the creep experiments, a constant load could be applied using discrete 15 g weights or an electromagnetic system for forces up to 2 kg. A silicon dummy was used to check that no spurious creep occurred at the specimen–glue interface with time, whatever the temperature of the measurement, over the entire range explored, 300 to 800 K.

## 3. The dependence of the initial resistivity on the bilayer period

The electrical resistance of the sample was first measured at a reference temperature of 300 K, in the as-sputtered condition. The corresponding resistivity values are plotted in

figure 1 as a function of the number of atomic planes per elemental silver or nickel stratum. The general trend is a progressive increase as the period is lowered. In fact, two series of data points are distinguished; they refer to measurements on multilayers prepared at room temperature or deposited on a substrate cooled at 100 K, respectively. The latter, represented by circles, lie on a curve of hyperbolic type. The former (square symbols) follow a similar variation profile but with values which are significantly smaller at the lowest periods. In contrast, in the limit of the largest periods, both series tend towards the same asymptotic level.

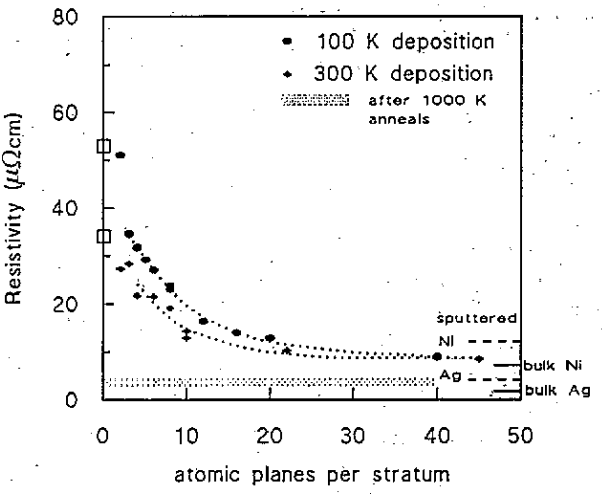


**Figure 1.** The variation of the resistivity as a function of the number of atomic planes per elemental stratum, in equiplane AgNi multilayers. The squares on the ordinate axis indicate the resistivity of co-sputtered AgNi films.

The rapid increase of resistivity observed at low periods originates mainly in the diffuse scattering of electrons at the interfaces. However, topological as well as chemical disorder within the strata may play a role too. In the present case of multilayers with grains of nanometric size, the high density of grain boundaries provides a further contribution to electron scattering. This is confirmed by considering the resistivities of pure Ag and Ni films prepared separately under the same conditions as the multilayers, which are much greater than those of the bulk elements. In fact, the unimetallic sputtered films have ultrafine grains of typical size some ten of nanometres. Here is the reason for their much greater resistivity relative to the bulk coarse-grained metals. This also explains the high asymptotic level for the multilayers, which lies well above that expected for the harmonic average of the resistivities of the constituent elements weighted by their respective thickness, assuming independently conducting layers and specular interfaces. However, if the resistivities of the sputtered pure metals are taken into the calculation rather than those of their coarse-grained counterparts, better agreement is obtained. More importantly, it should be noted that the grain boundary contribution depends on the period since, as already stated, the grain size becomes smaller as the period is decreased. This makes the deconvolution of the respective contributions of the two scattering processes, interface and grain boundary, difficult. Accordingly, hyperbolic variation laws of the type proposed by Fuchs [5] and Sondheimer [6] for thin films, or by Carcia and Suna [7], or else by Dimmich [8], are simple guidelines for the interpretation of the data.

The excess resistivity of the multilayers sputtered at 100 K is explained by considering that less relaxation takes place during the low-temperature deposition, with the result that larger elastic distortions and more topological disorder occur. In addition the grain size is then smaller.

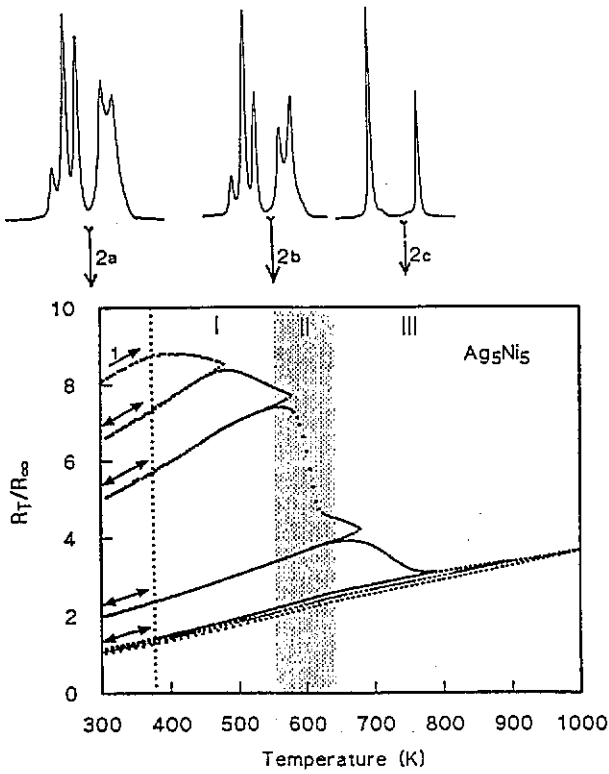


**Figure 2.** An evolution profile of the resistance as a function of temperature in a $Ag_5Ni_5$ multilayer submitted to heating and cooling runs at progressively increased temperatures. The x-ray spectra were obtained at 300 K from an identical sample taken in its as-sputtered state (*a*), or after anneals at 560 K (*b*) and 750 K (*c*).

The open symbols refer to non-stratified materials. Two samples were prepared by co-sputtering Ni and Ag targets with deposition at 300 K or 100 K. Their composition is the same as the global one of the equiplane multilayers. X-ray diffraction indicated an amorphous-like state for the latter. The corresponding resistivity is still higher than in the multilayered samples, on account of the existing topological and chemical disorder. For the nominally $Ag_3Ni_3$ (with 300 K deposition) or $Ag_2Ni_2$ multilayers, the structural state is close to that of the co-sputtered samples, with an eventual composition modulation.

Finally, all samples were heated up to 1000 K. It is shown in the next section that this treatment results in the loss of periodicity and in grain coursening. The resistivity of all the annealed samples was found to be roughly the same, whatever the initial bilayer period, lying between 3 and 4 $\mu\Omega$ cm, as represented by the shaded strip in the figure.

## 4. Resistivity profiles and annealing stages

We followed the temperature variations for the electrical resistivity to investigate the successive stages of the structural evolution which takes place during thermal treatments. The annealing sequence consisted of alternate heating and cooling runs at the rate of 2 K $min^{-1}$, at progressively increased temperatures. Figure 2 shows the observed profile

for a $Ag_5Ni_5$ multilayer. All the resistance values were referred to that in the fully annealed state. Three regions are distinguished. At first, resistivity varies linearly and reversibly in response to thermal scattering. Next, above about 380 K, a deviation from linearity appears. In this second region, which extends up to 560 K, the cooling runs back to ambient temperature clearly show that a non-recoverable resistivity decrease occurs. Its total amplitude reaches 30%. The constituent elements having negligible mutual solubility, it is likely that the temperature rise favours unmixing in the interfacial regions. Concomitantly, topological rearrangements are supposed to take place at the interfaces, these being sharper and more ordered, the more specular the electron scattering becomes. Hence the resistivity is decreased. This scheme is supported by the x-ray diffraction spectra recorded after annealing at 560 K, that is at the end of the stage considered, (figure 2(*b*)). The superlattice peaks look sharper than in the as-spluttered condition, (figure 2(*a*)). Magnetic measurements also suggest that the interfaces become chemically more abrupt. A second stage starts above 560 K, when a drastic resistivity drop shows up. The resistivity is then reduced by a factor of more than two. This stage corresponds to the loss of artificial periodicity, as shown unambiguously by the disappearance of the superperiodicity peaks in the x-ray spectrum. Then, an agglomerate of pure silver and pure nickel grains is formed. At still higher temperatures, a third stage takes place, until the final, equilibrium state is reached, at around 1000 K. The last stage reflects the progressive growth of the grains.

This pattern is typical of most real multilayers studied. For the sake of comparison, we have traced the resistivity profiles for the atypical cases of a co-sputtered AgNi sample already defined and a nominally $Ag_2Ni_2$ sample (see figure 3). As mentioned above, these samples are pseudo-amorphous, that is they both exhibit a high degree of topological disorder. A common feature of the corresponding profiles is that a very abrupt resistivity change occurs in a narrow temperature range centred on 360 K. The resistivity is then reduced by two. This rapid change corresponds to what can be called crystallization, using the terminology of amorphous metallic alloys. Further investigations are needed to examine the detailed evolution which proceeds on subsequent heating.

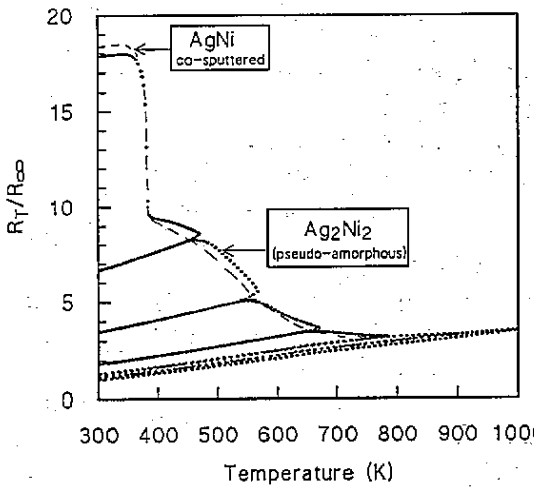


**Figure 3.** Resistance versus temperature in two pseudo-amorphous samples prepared by co-sputtering and alternate deposition of two atomic planes of silver and nickel, respectively. The two profiles look very similar, with a marked 'crystallization' stage at 370 K.

Pure Ag and Ni thin films obtained by sputtering were also studied. The excess resistivity associated with the presence of a dense array of grain boundaries is progressively eliminated

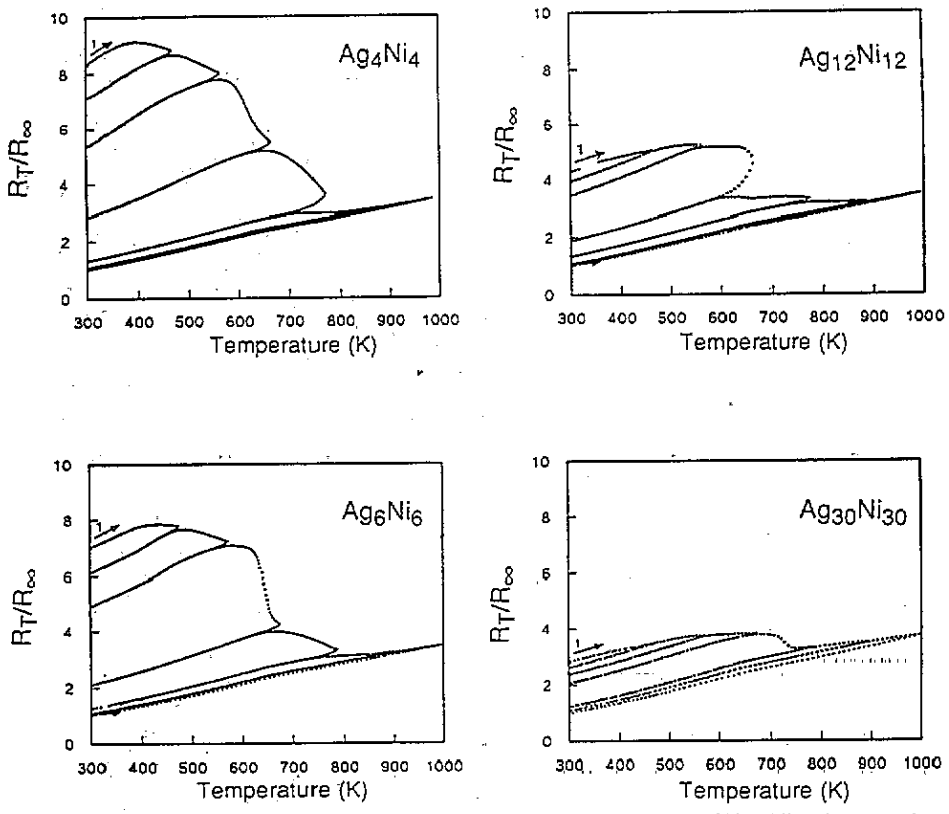


**Figure 4.** The influence of the bilayer period on the resistance profiles. All resistance values refer to that in the annealed state at 1000 K.

by anneals in the range between 300 and 800 K. The room temperature resistivity is then reduced by factors of approximately 2 and 1.5, respectively.

Figure 4 is a general picture of the various profiles observed when the period is varied. For all periods, the major features of the profile already described for the $Ag_5Ni_5$ multilayer are found again. An interesting aspect is the temperature location of the evolution stages revealed by these profiles. Figure 5 provides an overview of the general trends. For clarity, only the envelopes of the successive heating and cooling runs are represented. The broken curves are simply guides to delineate the beginning or the end of stages I and II.

A first remark is that stage I starts at approximately the same temperature, 380 K, for all periods. The fact that this stage begins at a relatively low temperature suggests that it corresponds to local reorganizations which do not involve long-distance diffusion. In other words, the underlying mechanism is simply interfacial relaxation. In contrast the second stage appears to be shifted towards higher temperatures for the higher periods. This is consistent with the idea that the destratification process responsible for this stage requires atomic transport over distances of the order of the bilayer period.

## 5. Evolution kinetics and related enthalpies

Measurements were also performed under isothermal conditions. The experimental procedure consists of a rapid temperature rise, to reach the selected temperature within a few seconds. Typical durations for the isotherms extend over several days.

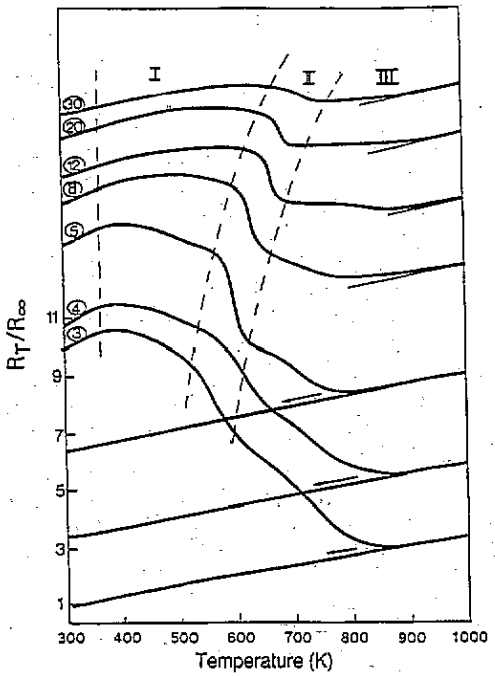


**Figure 5.** A summary of the resistivity profiles of AgNi multilayers for a broad range of bilayer periods. The figures in the circles indicate the number of atomic planes per elemental stratum. For clarity, only the envelopes of each set of heating and cooling curves are shown. All are represented at the same scale, but they are shifted vertically with respect to each other.

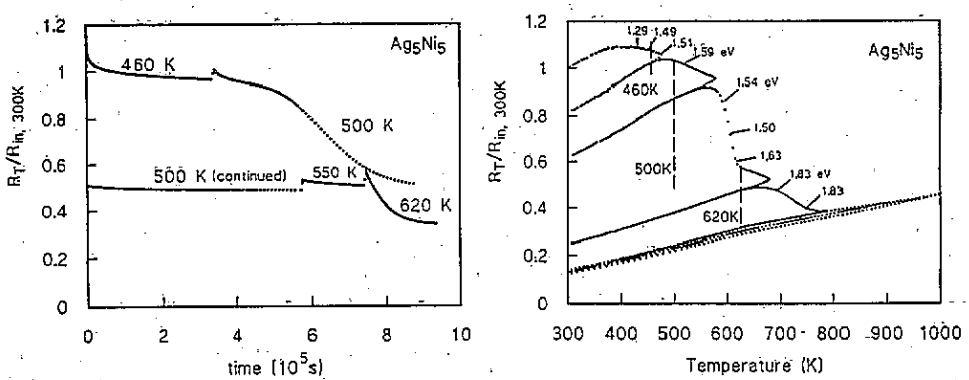


**Figure 6.** Left: the time evolution of the resistance, in $Ag_5Ni_5$, during successive isothermal anneals at 460 K, 500 K, 550 K and 620 K. For convenience, the final part of the 500 K isotherm and further sequences were plotted with reference to zero in the time scale. Right: the evolution of resistance with temperature, in another $Ag_5Ni_5$ sample submitted to heating and cooling cycles at a rate of 2 K $min^{-1}$. For a comparison, the vertical extent of the isothermal recovery (left figure) is represented by the broken lines. The measured activation enthalpies are reported on the figure to locate the degree of structural evolution to which they refer.

Figure 6 is illustrative of the observed kinetic behaviour. It refers to a $Ag_5Ni_5$ multilayer.

The left curves are isothermal variations traced during successive long-duration temperature steps at 460 K, 500 K, 550 K, and 620 K. The corresponding resistance drops are represented on the figure to the right, in the resistance versus temperature diagram, by the broken vertical lines. During the first temperature step at 460 K, the resistance decrease exhibits an exponential character. It tends slowly towards an asymptotic level. The only activated process is interfacial relaxation. When this stage is in its terminal phase, it is only increasing the temperature to 500 K that the second mechanism, the one responsible for the second stage, is triggered, at least at the time scale of the experiments. In this second part, the shape of the resistivity curve is totally different, since it is of sigmoidal type. Finally, after a marked slowing down of the reaction, the temperature was incremented further, until the onset of grain growth, at 620 K. The variation with time again looks exponential. In short, these experiments enable a better separation of the successive evolution stages. The corresponding processes appear to occur sequentially with little overlap and are characterized by differing kinetics. Similar isothermal experiments were also carried out on $Ag_4Ni_4$ and $Ag_{30}Ni_{30}$ multilayers. The evolution profiles look quite similar to those in $Ag_5Ni_5$, but the relevant temperatures are somewhat different. In $Ag_{30}Ni_{30}$, a temperature of 600 K is required to observe the sigmoidal profile characteristic of destratification.

To complement the kinetic study, it was interesting to determine the activation enthalpy of the underlying processes. This was done by using the change-in-slope method, with temperature steps of 20, 30 or 40 degrees. The relevant enthalpy, $H$, was derived from the slope ratio $s_2/s_1$, by the usual expression $H = k\ln(s_2/s_1)/(1/T_1 - 1/T_2)$, where $k$ is the Boltzmann constant [9]. Typically, ten to twenty such measurements were performed during the course of each stage. Average values obtained in a $Ag_5Ni_5$ multilayer are given in table 1, for the different temperature intervals. They are reported in figure 6, to show the degree of structural evolution to which they correspond. It is noticed that the activation enthalpies for the third stage are substantially larger than those for the first two stages.

**Table 1.** Activation enthalpies measured using the slope method for temperatures between $T_1$ and $T_2$ during the structural evolution of a $Ag_5Ni_5$ sample. The atom jump frequency was calculated for the mean temperature of each interval, taking $\nu_0 = 10^{14}$ s$^{-1}$.

| | Stage I | | | | Stage II | | | Stage III | |
|---|---|---|---|---|---|---|---|---|---|
| $T_1$ (K) | 410 | 430 | 450 | 490 | 550 | 570 | 590 | 670 | 700 |
| $T_2$ (K) | 430 | 450 | 470 | 510 | 570 | 590 | — | 700 | — |
| | | | 490 | | | | 670 | | 750 |
| $H$ (eV) | 1.29 | 1.49 | 1.51 | 1.59 | 1.54 | 1.50 | 1.63 | 1.83 | 1.83 |
| $\nu$ (s$^{-1}$) | 0.03 | 0.001 | 0.006 | 0.01 | 1.4 | 8.7 | 7 | 4 | 7 |

One has to realize that the measured enthalpies are but effective values, due to the intricate structure and resulting complexity of the kinetics. Several complicating factors are expected to play a role, such as the existence of a hierarchy in the various diffusional processes, dislocation, interfacial, grain boundary or bulk. A broad spectrum of atom jump rates is likely to exist too, on account of the elastic distortions and diversity of the local atomic environments. Nevertheless some remarks can be made.

In stage 1, the activation enthalpy is gradually increased as the reaction proceeds. This explains why the atom jump frequency, $\nu$, remains low. A rough estimate, using the relation $\nu = \nu_0 e^{-H/kT}$ and assuming $\nu_0$ to be constant at a value of $10^{14}$ s$^{-1}$ yields an atom jump rate of about $10^{-2}$ s$^{-1}$, in the whole temperature range concerned, although this range is very broad. This behaviour is to be interpreted in the light of the length

results presented in the second part of this paper. Namely, the fact that the atomic mobility is progressively reduced on annealing is well explained if one considers the substantial densification evidenced during the interface relaxation. This densification results in a rise of the enthalpy barriers for atomic motion. The eventual reorganization movements, more or less cooperative in nature, which do not necessarily imply enthalpy jumps, are themselves made more difficult. In the destratification stage, the enthalpy varies very little. The atomic jump frequency appears to be much higher, of the order of 10 jumps per second. Atomic transport can then proceed at an enhanced rate. Lastly, in the region of grain growth after destratification, the activation enthalpy is much higher. The evolution of the grain boundaries towards lower-energy boundaries, and their probable enrichment in the solute element, tends to hinder the relevant atomic mobility.

**Table 2.** Main pre-exponential factors and activation enthalpies for atomic diffusion in coarse-grained silver and nickel. Most of these data are found and discussed in the book by Kaur and Gust [10].

| Diffusion process | | $D_0$ ($cm^2\ s^{-1}$) | $H$ (eV) | Reference |
|---|---|---|---|---|
| Volume (self-diffusion) | Ni | 0.92 | 2.88 | [11] |
| | | 1.82 | 2.95 | |
| | Ag | 0.04 | 1.76 | [11] |
| Ag | along dislocations | 0.14 | | [12] |
| | Grain bounday (800–900 K) | 0.03 | 0.86<br>0.88 | |
| $Ni^{63}$ in Ag along dislocations (900–1100 K) | | $8.5 \times 10^{-7}$ | 1.25 | [14] |
| Ag in Ni volume (1300–1700 K) | | 9.0 | 2.89 | [14] |

The measured enthalpies are to be compared with those in bulk silver and nickel. A few reference values for the various diffusional mechanisms are listed in table 2. Clearly, for AgNi in the multilayered condition, the activation enthalpy lies well below the enthalpy for self-diffusion in the constituent metals. It appears that the diffusion of silver in bulk nickel is totally excluded in the temperature range of stage 1. Conversely, nickel might be a rapid diffuser in silver, at least along dislocation lines. In fact, a high density of misfit dislocations exists in the stratified structures under study. However, the dislocation lines lie in the plane of the interfaces and cannot favour transverse diffusion. In contrast, the grain boundaries are perpendicular to the interfaces and thus can act as efficient diffusion channels for the destratification process.

## 6. Densification effects

Length profiles were traced during the course of the temperature cycles, similar to those for the resistivity study. Figure 7 displays the observed profiles for length and resistivity, for a

$Ag_8Ni_8$ multilayer. Concerning the length variations, a remarkable feature is the appearance of a substantial contraction during the anneals. The total effect, measured at the reference temperature of 310 K, amounts to about $6 \times 10^{-3}$.

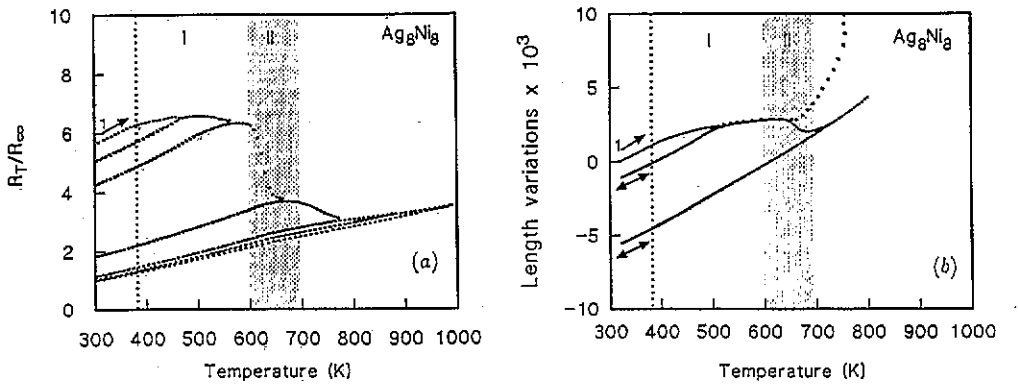


**Figure 7.** Resistivity and length profiles recorded during successive heating and cooling runs in $Ag_8Ni_8$ multilayers. For the length measurements, two very different conditions were used: (*a*) minimum load (full curve), apart from thermal expansion, only a contraction effect is detected; (*b*) 30 g load (dotted curve), a dilational creep effect shows up, but only in the destratification stage labelled II (cf section 7).

A more detailed inspection of the two plots reveals that two main stages, labelled I and II in the figure, can be distinguished in the length profile. Very strikingly, the length variations reproduce the observed structure of the resistivity variation curves. A neutral region in the sense of the structural evolution is first noted, below about 380 K, when the material expands linearly and reversibly under the action of anharmonic vibrations. It is followed by stage I, in which a substantial contraction progressively takes place over a broad temperature range. Finally, above 600 K, a drastic contraction shows up, concurrently with the dramatic resistivity decrease associated with destratification.

In the first stage, that we assigned to interfacial relaxation, a contraction of $3 \times 10^{-3}$ takes place. This contraction originates in local rearrangements which imply topological short-range ordering. These reorganizations are accompanied by the elimination of the excess free volume associated with the disordered state and quite likely by the elimination of excess vacancy defects. To illustrate the importance of this effect, it is recalled that the amplitude of the contraction is of the same order as that reported in many amorphous metal–metal alloys as a result of the so-called structural relaxation in these materials and subsequent crystallization. Next to interfacial relaxation, destratification results in a further contraction with comparable amplitude.

Isothermal length measurements were also performed. Figure 8 displays in parallel the evolution of resistance and length during comparable isothermal anneals. It is seen that the form of the kinetics for the length variations look very similar to that of resistance, namely exponential in the region of interfacial relaxation and sigmoidal during destratification.

## 7. Anelastic and diffusional creep

A series of creep experiments was also carried out by submitting the films to uniaxial tension by application of a constant (30 g) load. The corresponding profile for a $Ag_8Ni_8$ sample

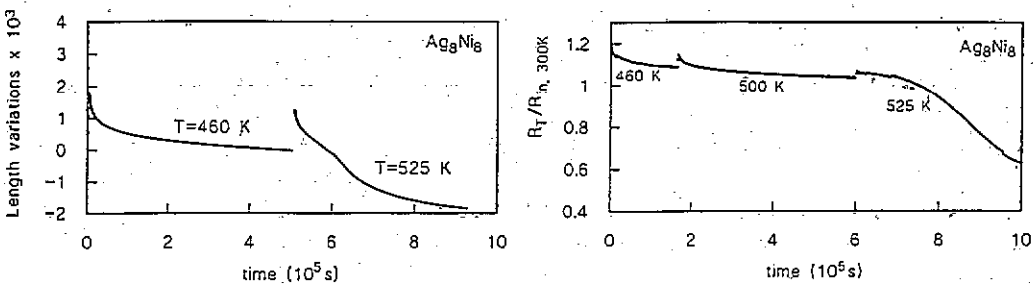


**Figure 8.** The comparative evolution of resistivity and length with time, during various isothermal anneals, in $Ag_8Ni_8$ multilayers.

identical to the one used for the dilatometric study is also plotted in figure 7, as a dotted curve. It is apparent in the figure that the early part of the curve is superimposed on the one for the unloaded sample. A substantial contraction is again detected. It is only in the destratification region that the two curves differ in shape, namely, in this region, a sudden upturn is detected and the trend is towards a marked expansion. This is likely to be due to the onset of diffusional creep. It is not unexpected that creep is activated at the same time as destratification manifests itself, since they both require substantial atomic diffusion. As soon as the atomic mobility becomes substantial, the two processes start operating concurrently.

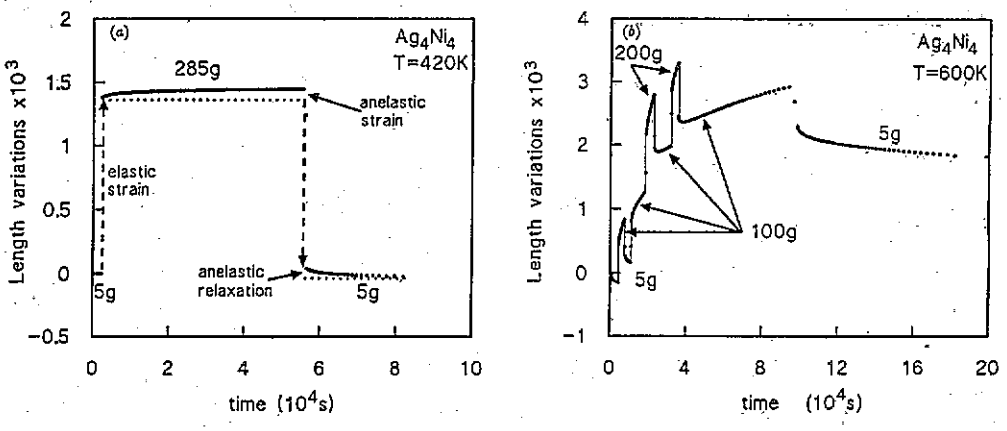


**Figure 9.** Length variations measured in $Ag_4Ni_4$ submitted to uniaxial stress. The left-hand curves ($a$) were traced during an isotherm at 420 K, in the region of interfacial relaxation. The right-hand curves, ($b$) are for various applied loads at a constant temperature of 600 K, that is when destratification proceeds in unloaded samples.

In order to show that this diffusional creep can develop only at temperatures above those of stage I, we have studied the length variations under a greater uniaxial load of, 100, 200 or 285 g. This was done during isothermal anneals in either stage of the microstructural evolution. The multilayer considered is $Ag_4Ni_4$. Figure 9($a$) illustrates the behaviour of the film at 420 K. In response to the application of the 190 MPa stress, an instantaneous, that is elastic, strain response is observed, amounting to $1.4 \times 10^{-3}$. This corresponds to a value of 136 GPa for the Young's modulus, which is in good agreement with earlier determinations [4, 15]. This response is followed by a delayed strain which develops progressively and tends towards an asymptotic value. The amplitude of this relaxation stays below a few per cent of the elastic response. On unloading, a converse relaxation allows full recovery of the

initial length. This reversible behaviour is characteristic of anelastic creep. In bulk metallic materials, it is attributed to a dislocation glide.

When the temperature of the experiment is located within the destratification region, (figure 9(*b*)) a totally different behaviour is noted. On application of a 100 g or 200 g load, by successive steps, creep is the dominant evolution; the higher the load, the larger the rate. The essential feature is that when load is released (down to a value of a few grams only), some recovery takes place, similar to the case of anelastic creep, but this time it is limited to a small fraction of the length increase. Stated differently, most of the strain associated with the creep process is not recovered. This is definite evidence that diffusional creep operates.

A more general view of the contraction and creep effects and their dependence on the bilayer period is provided by figure 10. All the films were loaded with a mass of 30 g during the whole duration of the temperature cycles. The onset of destratifaction is unambiguously revealed by the advent of a dilational creep effect. Thus, the contraction measured prior to creep only refers to the effect of interface relaxation, stage I. It is noticeable that the amplitude of the contraction is rapidly decreased as the period is increased. For instance, in $Ag_{12}Ni_{12}$, it is reduced to below $1 \times 10^{-3}$. As soon as the periodicity reaches 16 atomic planes per elemental stratum, only a minute contraction is detected, if any. This trend is not surprising since this effect is expected to vary, to a first approximation, as the interface density. A final remark is that, just like for resistivity stage II, the beginning of creep is progressively shifted towards higher temperatures as the period increases.

Finally, it is noted that, in the $Ag_2Ni_2$ sample, with dominant pseudo-amorphous character, a marked contraction accompanies the 370 K resistivity stage linked to crystallization (cf figure 3). As far as creep is concerned, it starts much earlier than in the multilayers. This behaviour is comparable to that of unimetallic nanocrystals, which were found to give rise to very early viscoplastic flow.

## 8. Concluding remarks

The several approaches followed, resistometric, dilatometric and creep, enabled a detailed analysis of the successive steps of the microstuctural evolution of the AgNi multilayers studied to be carried out. They brought some quantitative information about the densification which intervenes during interfacial relaxation and destratification. The kinetic parameters for these processes were also determined and the corresponding atomic mobility was inferred.

Concerning the densification effects, a straightforward comparison can be made between the metallic multilayers, on the one hand, and the amorphous metallic alloys, on the other hand. Both form out-of-equilibrium systems with a double metastability. The initial amorphous state is metastable with respect to the ideal glass and also to the crystal. The primitive interfaces of the multilayers exhibit a metastable character with respect to a relaxed configurational state of lower energy. Moreover, as a whole, the stratified state is metastable with respect to a conventional, three-dimensionally periodic structure.

On heating, as soon as the atomic mobility becomes large enough, the two types of artificial structures evolve towards thermodynamical equilibrium via intermediate states: the glass undergoes so-called 'structural relaxation' before crystallization occurs. The multilayers give rise to interfacial relaxation before destratification.

Every one of these structural modifications is accompanied by a substantial densification indicative of the elimination of excess volume. There exists a common reason that multilayers and metallic glasses possess a large volume excess. In metal–metal amorphous alloys, for amorphization requirements, the two constituent elements always have a large size

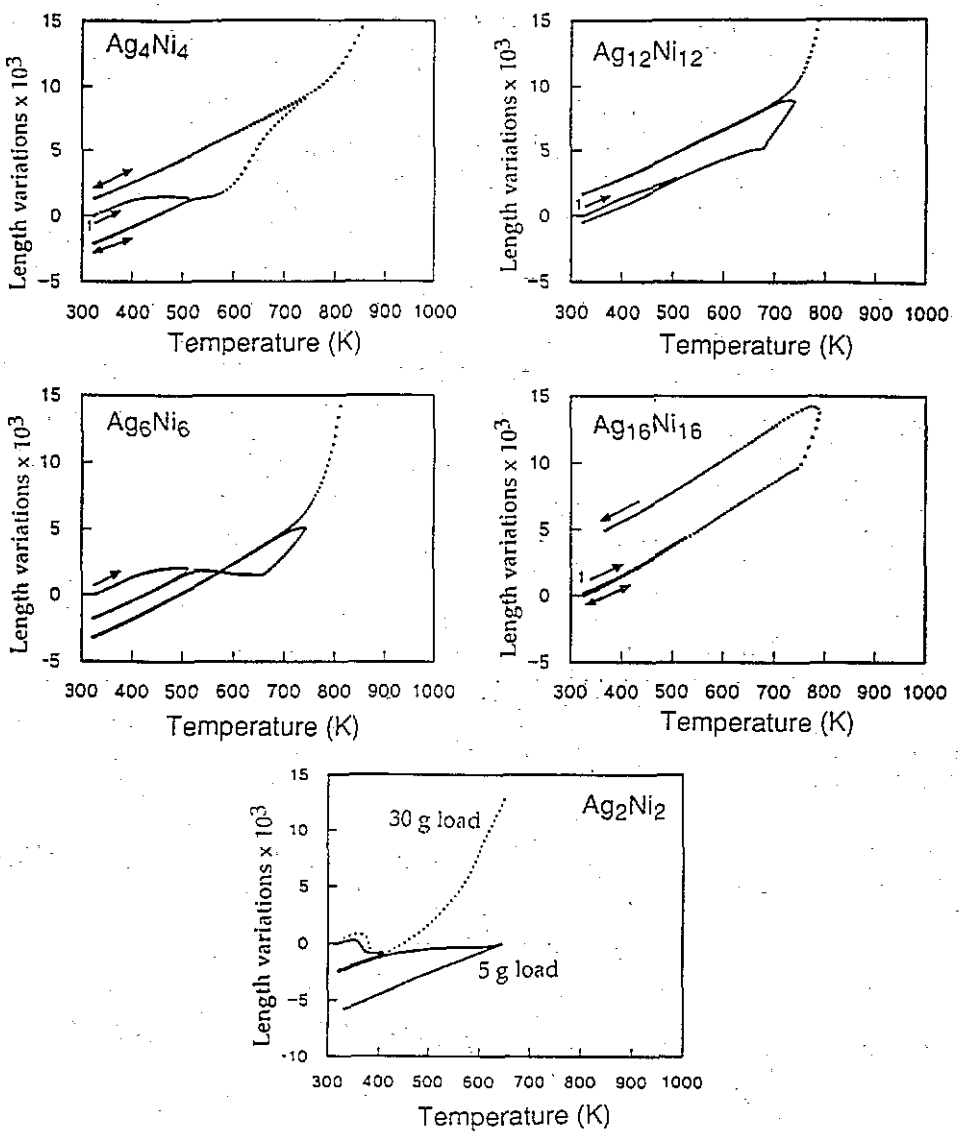


**Figure 10.** Length variation profiles in AgNi multilayers of period 4, 6, 12, and 16 atomic planes per elemental stratum. All the films studied were loaded with 30 g. (For a comparison consider figure 7 for the $Ag_8Ni_8$ sample.) The lower curve displays the behaviour of two non-stratified $Ag_2Ni_2$ samples: one was exposed to a minimum load, to avoid creep, while the other was submitted to a 30 g load.

difference. Similarly, the multilayers with strained layers under consideration are composed of two elements with large lattice mismatch. Here lies the main cause for the magnitude of the excess volume. In the glassy alloys it is termed free volume. It is generally considered to be distributed since it is linked to the chemical and topological disorder, but it can be localized in the form of quasi-vacancies. Total densification after crystallization amounts to about one per cent. In the multilayers with large size mismatch, as is the case for the AgNi multilayers, the excess volume originates in the interfacial disorder and also in the large

density of grain boundaries. We have shown that the total amplitude of the densification is of the same order of magnitude, at least at the smaller periods, as in amorphous metallic alloys.

The analogy could be continued by commenting on the annealing kinetics. In structural or interfacial relaxation, the kinetics tends to obey logarithmic laws in the time scale. These are explained in either case by the presence of an extended spectrum of relaxation rates, and also by the rise of enthalpy barriers as the reaction proceeds.

## Acknowledgments

The help of G Casali, C Mairy and A Pierrot in the preparation of the samples and realization of the experiments is gratefully acknowledged. Helpful discussions with A Chamberod and Ph Gerard were also greatly appreciated.

## References

[1] Rodmacq B 1991 *J. Appl. Phys.* **70** 4194
[2] Rodmacq B and Thibault J 1991 *Mater Res. Soc. Symp. Proc.* **97** 229
[3] Dos Santos C A, Rodmacq B, Vaezzadeh M and George B 1991 *Appl. Phys. Lett.* **59** 126
[4] Pelosin V, Rodmacq B, Hillairet J, Carlotti G, Fioretto D and Socino G 1993 *Internal Friction and Ultrasonic Attenuation in Solids* (Zurich: Trans Tech Publishing) p 359
[5] Fuchs K 1938 *Proc. Camb. Phil. Soc.* **34** 100
[6] Sondheimer E H 1952 *Adv. Phys.* **1** 1
[7] Carcia P F and Suna A 1983 *J. Appl. Phys.* **54** 2000
[8] Dimmich R 1985 *J. Phys. F: Met. Phys.* **15** 2477
[9] Damask A C and Dienes G J 1963 *Point Defects in Metals* (New York: Science)
[10] Kaur L and Gust W 1989 *Handbook of Grain and Interphase Boundary Diffusion Data* (Stuttgart: Ziegler)
[11] Peterson N L 1978 *Properties of Atomic Defects in Metals* (Amsterdam: North-Holland) p 4
[12] Turnbull D and Hoffman R E 1954 *Acta Metall.* **2** 419
[13] Hoffman R E and Turnbull D 1951 *J. Appl. Phys.* **22** 634
[14] Vladimirov A B, Kaigorodov V N, Klotsman S M and Trakhtenberg I Sh 1979 *Phys. Met. Metallogr.* **48** 352
[15] Pelosin V 1993 *Thesis* University of Grenoble
[16] Chamberod A, Chambron W and Hillairet J 1983 *Les Amorphes Metalliques* (Paris: Les Editions de Physique) p 329